Preventing Downhole Tool Failure During Geothermal Well Construction Using a Hybrid Real-Time Temperature Management Advisory System

Naveen Velmurugan and Sadjad Naderi

Virgil Dynamics SAS

Pradeepkumar Ashok and Michael Yi

Intellicess, Inc.

Keywords

Geothermal wells, Drilling, Hydrothermal model, Real-time prediction

ABSTRACT

Drilling cost-efficient, safe, and deep wellbores is key to scaling geothermal energy. However, the elevated costs associated with high non-productive and invisible loss times (NPT/ILT) are taxing on the operators, acting as a severe bottleneck in utilizing geothermal energy. In deep geothermal wells, the leading contributors to NPT/ILT are the failure of downhole tools and/or absence of their measurements.

Continuous downhole parameter measurements are often hindered by mud circulation interruptions or downhole tool failures caused by high operating temperatures. During drilling operations, the mud temperature fluctuates due to its thermal interaction with the surrounding environment, which is typically hotter. This variability is particularly pronounced during activities such as connection and tripping, when mud circulation and downhole measurements are unavailable. Estimating temperature distribution along the wellbore before deploying costly downhole tools is critical to mitigate the risk of failure. Furthermore, developing an effective strategy to cool the mud relies on factors including circulation rate, duration, and inlet mud temperature.

In this study, we introduce an approach that combines physics-based modeling and machine learning techniques to achieve real-time prediction of mud temperature distribution. This method aims to enable precise and continuous estimate of mud temperature along the wellbore, facilitating more efficient well thermal management. An automated calibration system tailored for adjusting parameters within the physics-based hydrothermal model was also developed. This calibration process is designed to enhance the accuracy of the model and further improve the performance of the monitoring system. The calibration system is smartly triggered by Discrete Event Simulation (DES) technique as and when operational conditions change on the rig. The advisory system synergizes with the monitoring system to suggest optimal mud circulation durations and flow rates.

These recommendations are tailored to the inlet mud temperature, thereby ensuring precise control over the targeted temperature profile within the wellbore.

Our approach has been validated using select cases from the Utah FORGE dataset for which wellbore temperature measurements were available. Our real-time monitoring system was able to estimate the mud temperature profile along the wellbore after prolonged stagnation of mud inside the wellbore due to other operations like connection and tripping when bottom hole mud temperature measurements were absent. The automatic calibration technique proved efficient in updating uncertain model parameters to provide improved predictions. Ultimately this approach can drastically improve temperature monitoring and management during the construction of a geothermal well and reduce tool failure.

1. Introduction

Geothermal energy is one of the leading candidates for providing a clean energy infrastructure. However, drilling deep wells to extract necessary heat energy poses a distinctive challenge: the intense temperatures encountered during the exploration of deep underground reservoirs. During the drilling process, drilling mud – an engineered fluid – is circulated through the drill string and up to the surface through the annulus. Drilling mud is essential to maintain pressure inside the wellbore, removal of rock cutting and lubrification, among others. They also act as a conduit for mud pulse telemetry (MPT) for data transmission while drilling from the expensive downhole tools. However, the elevated temperatures encountered in geothermal wellbores lead to increasing wear and tear of downhole tools (Mitchell & Miska, 2011) and thus elevating the risk of tool failure (Kruszewski & Wittig, 2018) leading to lack of critical wellbore information for an efficient drilling operation.

Estimating bottom hole temperature is paramount in geothermal wellbore construction and numerical simulations using finite element models (FEMs) and finite difference methods (FDMs) can be utilized, but their computational burdens often limit their real-time application (Chen & Novotny, 2003). Reduced order models such as analytical models (Hasan & Jang, 2021) and semi-analytical models (Polat, 2022) offer reduced computation effort but compromises on accuracy due to simplifying assumptions that overlook crucial factors like complex wellbore geometries and transient thermal behaviors. Data-driven machine learning (ML) models pose certain drawbacks such as heavy reliance on data quality that are generally lacking and their transferability to new scenarios can be challenging (Kshirsagar & Sanghavi, 2022). An improved approach is necessary to overcome the current approaches requiring static input requirements rendering them impractical for real-time decision-making during a dynamic drilling operation (Gonzalez Angarita, 2020) where the rig states and operational parameters (mud flow rate, drill string rotation, location of bit with respect to hole depth, etc.) change quite frequently. In this study, a Physics-Informed Machine Learning (PIML) model is proposed offering a combination of physics-based FDM model (Hasan, Kabir, & Sarica, 2018) with real-time data suitable for predicting mud temperature distribution along the wellbore.

The strength of using FDM models in simulating heat transfer within wellbores lies in discretizing the wellbore geometry into a grid, allowing for the precise evaluation of heat conduction, convection, and radiation across each individual point (Holmes & Swift, 1970) by considering influencing factors like fluid flow dynamics, formation properties, and frictional heating (Zhang, Xiong, & Guo, 2018). The resulting temperature profiles offer detailed insights into the thermal

landscape within a wellbore (Zhou, 2013). However, FDM models rely heavily on accurate input parameters, including rock and material thermal properties, fluid rheology (Merlo, Maglione, & Piatti, 1995), and wellbore geometry (Hasan, Kabir, & Wang, 2009). In reality, the input parameters come with significant uncertainties due to limited downhole measurements and indirect measurements from historical drilling operations, introducing potential discrepancies between the model predictions and real-world temperature profiles. Although computationally expensive, calibrating these models is necessary, commonly based on iterative trail-and-error approaches, until the simulated temperature profiles match the measured values at certain locations, like mud temperature at the wellbore outlet (Tekin, 2010). In this work, a calibration technique suitable for geothermal wellbore temperature estimation that is computationally efficient for real-time applications is utilized. The hydrothermal model presented in the next section was introduced in Naderi et al., 2024 and repeated here for improved readability.

2. Hydrothermal model

2.1 Governing equations

The borehole is modeled to capture thermal interactions between the wellbore and the surrounding rocks. The model is built on the following key assumptions: (i) the drilling fluid is treated as incompressible, maintaining constant density, specific heat capacity, and thermal conductivity; and (ii) the velocity of the drilling fluid inside the drill string and annulus is considered solely in the axial direction, while the radial velocity is disregarded. Governing equations (1) to (5) describe the heat flow in the fluid inside the drill string, the drill string pipe, the fluid in the annular space, the first layer of casing, and the casing/cement/surrounding formation, respectively and are detailed in the literature (Zhang, Xiong, & Guo, 2018).

$$-\frac{\partial(\rho_1 c_1 v_p T_1)}{\partial z}+\frac{2h_1(T_2-T_1)}{r_1}+\frac{q_p}{\pi r_1^2}=\frac{\partial(\rho_1 c_1 T_1)}{\partial t} \tag{1}$$

$$\frac{\partial}{\partial z}\left(\frac{\lambda_p \partial T_2}{\partial z}\right)+\frac{2h_2(T_3-T_2)r_2}{r_2^2-r_1^2}-\frac{2h_1(T_2-T_1)r_1}{r_2^2-r_1^2}=\frac{\partial(\rho_2 c_2 T_2)}{\partial t} \tag{2}$$

$$\frac{\partial(\rho_3 v_a c_3 T_3)}{\partial z}+\frac{2h_3(T_4-T_3)r_3}{r_3^2-r_2^2}-\frac{2h_2(T_3-T_2)r_2}{r_3^2-r_2^2}+\frac{q_a}{\pi(r_3^2-r_2^2)}=\frac{\partial(\rho_3 c_3 T_3)}{\partial t} \tag{3}$$

$$\frac{\partial}{\partial z}\left(\lambda_4\frac{\partial T_4}{\partial z}\right)+\frac{2h_3(T_5-T_4)}{r_4^2-r_3^2}-\frac{2h_3(T_4-T_3)r_3}{r_4^2-r_3^2}=\frac{\partial(\rho_4 c_4 T_4)}{\partial t} \tag{4}$$

$$\frac{\partial}{\partial z}\left(\lambda_i\frac{\partial T_i}{\partial z}\right)+\frac{1}{r}\frac{\partial}{\partial r}\left(\lambda_{effective}^{i,\,i+1} r\frac{\partial T}{\partial r}\right)=\frac{\partial(\rho_i c_i T_i)}{\partial t} \tag{5}$$

Here, r and z denote radial and axial coordinates, respectively. In Equations (1) to (4), the subscript numbers follow the layer order illustrated in Figure 1a, while the subscript i in Equation (5) denotes the layer number in casing/cement/surrounding formation. While a constant spacing is considered in the axial direction, a gradually increasing mesh is considered in the radial direction, whose schematic is shown in Figure 1b.

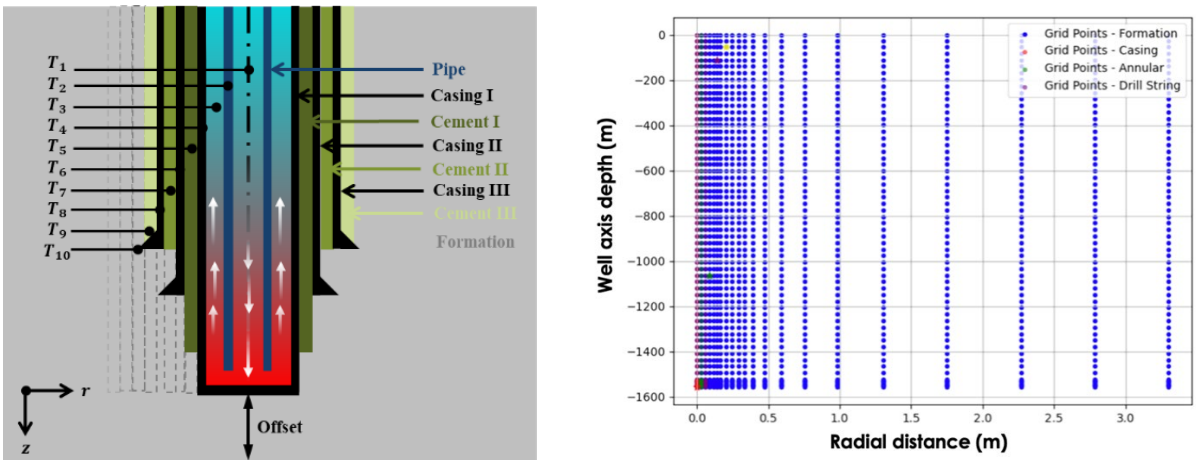

(a) (b)

Figure 1: (a) 2D schematic of a coaxial borehole heat exchanger, and (b) schematic of a 2D cross section through 3D model of the discretization of FDM grid. (Adapted from Naderi et al., 2024.)

In the context of the equations, T, h, λ, c and ρ represent temperature, convective heat transfer coefficient, thermal conductivity, specific heat capacity, and density, respectively. The conductivity coefficient between layer i and $i+1$, denoted as $\lambda_{effective}^{i,i+1}$, is calculated using the thermal-electrical analogy (Brown, Cassidy, Egan, & Griffiths, 2021), employing the following formulation:

$$R_{effective} = \frac{1}{\lambda_{effective}}, \quad R_{effective} = R_i + R_{i+1} = \frac{1}{\lambda_i} + \frac{1}{\lambda_{i+1}} \tag{6}$$

This expression signifies that the thermal resistivity of the effective layers can be considered analogous to electrical resistivity in series. The next section details the calculation of q_p and q_a, representing friction-induced heat source in drilling pipe and annular, respectively.

2.2 Source terms

The calculation of the friction-induced heat source involves considerations of fluid dynamics within the drilling pipe and the annulus (Zhang, Xiong, & Guo, 2018). Numerous empirical and analytical models exist for this purpose. Here, the Reynolds number (Re) as a crucial parameter is defined as (Durst & Arnold, 2008):

$$Re = \frac{\rho v D_h}{\mu} \tag{7}$$

where μ is the dynamic viscosity of the mud, and D_h and v are the hydraulic diameter and fluid velocity respectively. It should be noted that for the annular flow, $D_h = 4\,(d_3^2 - d_2^2)/(d_3 + d_2)$, where d_3 represents the diameter of the wellbore, and d_2 is the outer diameter of the drill string. For laminar flow ($Re \leq 2000$), the coefficient of friction resistance (f) is calculated as:

$$f = \frac{16}{Re} \tag{8}$$

In turbulent flow ($Re > 2000$), f is determined using the empirical Darcy friction factor equation:

$$\frac{1}{\sqrt{f}} = 4\log\left(Re\sqrt{f}\right) - 03.95 \quad (9)$$

The frictional resistance pressure drop in the drill string is then computed using:

$$\frac{\Delta P}{\Delta L} = \frac{2f\rho v_p^2}{d_1} \quad (10)$$

where L denotes the flow distance of drilling fluid. Similarly, in the annular region, the pressure drop is determined by:

$$\frac{\Delta P}{\Delta L} = \frac{2f\rho v_a^2}{d_3 - d_2} \quad (11)$$

Finally, the heat source term (q) in Equations **(1)** and **(3)** is quantified by:

$$q = \frac{\Delta P Q}{\Delta L} \quad (12)$$

where Q is the volumetric flow rate of drilling fluid.

2.3 Boundary and initial conditions

The initial temperature in the formation is determined by a linearly increasing geothermal gradient (G). Although a linear, continuous relationship is assumed, adjustments like including stepwise changing G can be made in the assimilation process, as discussed later in the following sections.

The inlet temperature is known and can be measured directly on the ground:

$$T_1(z = 0, t) = T_{in} \quad (13)$$

At the bottom of the well, the annulus drilling fluid temperature is equal to the drilling fluid temperature inside the drill string and the drill string temperature:

$$T_1(z = z_f, t) = T_2(z = z_f, t) = T_3(z = z_f, t) \quad (14)$$

where z_f is the vertical depth at the bottom of the well. There is no heat exchange between the formation and the atmosphere at the surface:

$$\frac{\partial T}{\partial z}\Big|_{z=0} = 0 \quad (15)$$

The formation temperature far away from the wellbore is undisturbed and is equal to the initial formation temperature. This condition is described at r_f, the end of the rock domain in the radial direction:

$$\frac{\partial T}{\partial r}\Big|_{r \to r_f} = 0 \quad (16)$$

2.4 Numerical solution

An implicit numerical method is implemented for the FDM employed in this work. Details of the implementation are adapted from (Zhang, Xiong, & Guo, 2018). This in contrast with the authors' earlier work (Naderi et al., 2024) where an explicit numerical scheme was implemented. The current approach is preferred for issues related to numerical stability while handling the real time data – streaming from the electronic drilling recorder (EDR) and/or the mud logging units. The FDM employed in this work for solving the governing equations utilizes a first-order forward difference scheme for temporal discretization and a central difference scheme for spatial discretization.

2.5 Sensitivity and observability

The primary objective of this work is to estimate the bottom hole temperature during geothermal drilling operations to better protect the downhole tools from thermal failures. The aforementioned hydrothermal model is dependent on several input parameters with high uncertainties and their perturbations can cause large impact on the estimation of bottom hole temperature. Thus, a preliminary sensitivity analysis is carried out. Since, geothermal gradient is not accurately known a priori to drilling a well, its sensitivity is numerically studied through trail-and-error approach. Two different scenarios are considered in this study: short circulation duration of about 3 hours (see Figure 2) and long circulation duration of about 2 days (see Figure 3). In addition, during the short circulation scenario, the geothermal gradient was changed at half-time, i.e., from 0.02 to 0.4 at 1.5 hours of circulation. The simulation parameters for this analysis are provided in Table 1. In all scenarios, the following observations hold:

1. The wellbore temperature profile is strongly dependent on the initial geothermal gradient. Any nominal variations in the gradient does not affect the bottom hole temperature estimation. Thus, initial model calibration when the required information is available or extracted from the real time data plays a crucial role in utilization of the hydrothermal model for temperature management system.
2. For a given variation in the geothermal gradient, changes in the outlet mud temperature were insignificant and changes in the bottom hole temperature were only slightly better. This leads to our hypothesis that geothermal gradient is not *observable* when only surface temperature is considered as the system measurement and bottom hole temperature is a necessary measurement during the calibration process.

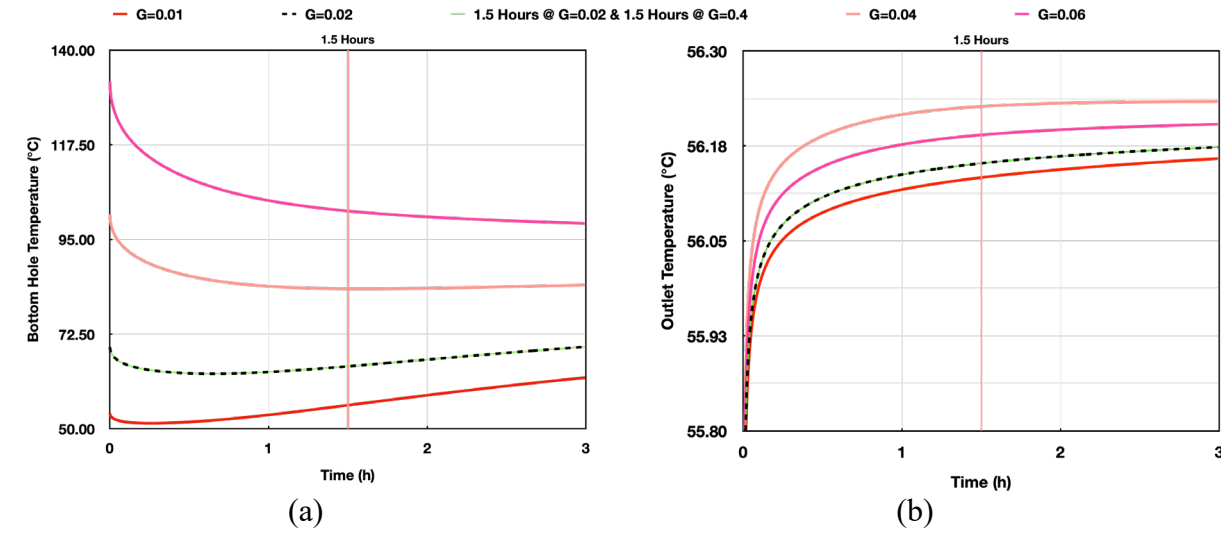

(a) (b)

Figure 2. Evolution of the bottom hole temperature (a) and the mud outlet temperature at the surface (b) during a short circulation scenario of 3 hours, for various geothermal temperature gradients (G). Changing G from 0.02 to 0.4 at 1.5 hours of circulation time shows no variation in the temperature evolution for both the parameters.

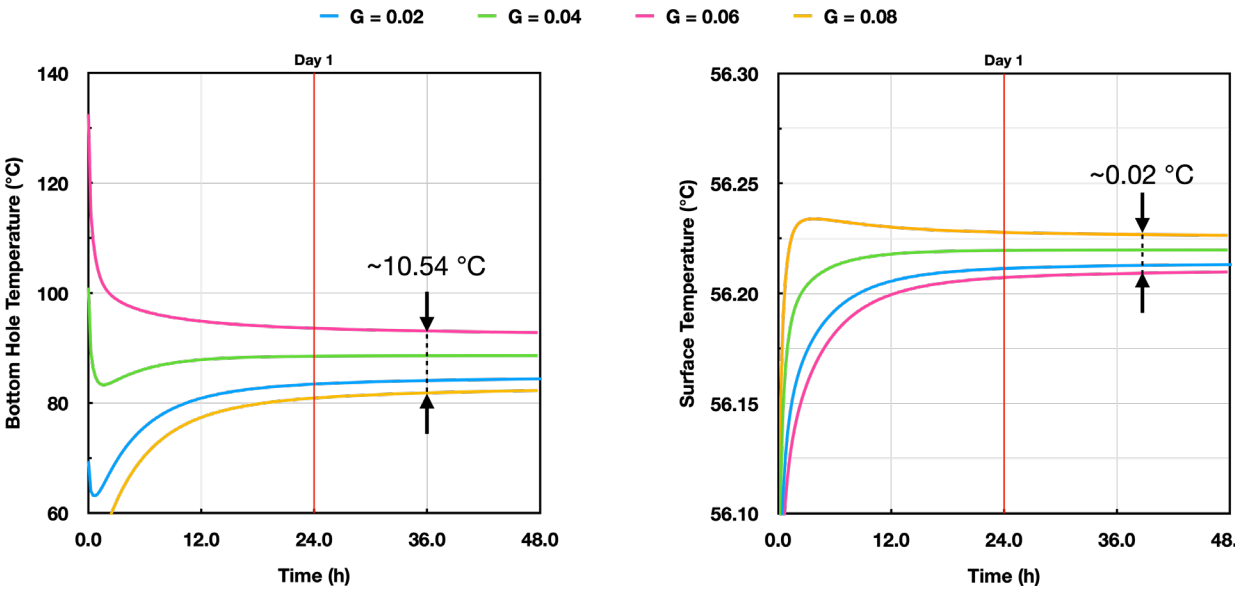

(a) (b)

Figure 3. Evolution of the bottom hole temperature (a) and the mud outlet temperature at the surface (b) during a long circulation scenario of 2 days, for various geothermal temperature gradients.

3. Model validation using UTAH Forge dataset

3.1 Data handling and calibration technique

As schematically illustrated in Figure 4, this engine comprises two distinct compositions, as already introduced in Naderi et al., 2024.:

1. **Static Data-Based Model:** This model component provides the initial condition to the dynamic model. When necessary, steady state solution can be utilized to transit to the transient simulation of the wellbore thermal dynamics. Since this segment is independent of considering input data in real-time, the choices for simulation time-step and techniques like implicit or explicit approach are open but must be suitably chosen to align with the thermal system's overall dynamics.

2. **Dynamic Data-Based Model:** Starting from the static-data based model simulation results as its initial condition, this model segment integrates live measurements into its simulation. Data assimilation, a critical process fusing observations with model predictions is operational to integrate real-time measurements and dynamics. The time step for this dynamic model aligns directly with the data frequency (here, 1 second) of the thermal-hydro model, ensuring continuous synchronization with real-time conditions.

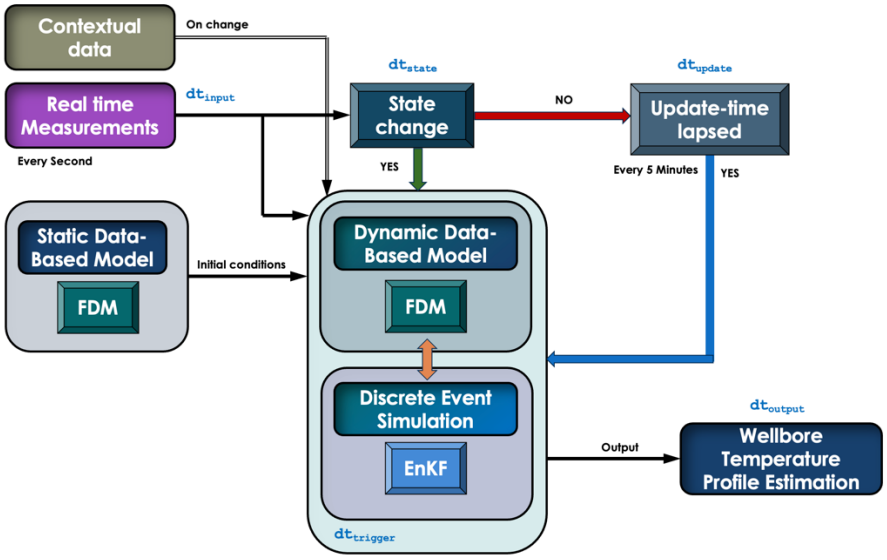

Figure 4: Schematic representation of the integrated framework, illustrating the dynamic assimilation of real-time data into the forward-marching explicit numerical solution. (Adapted from Naderi et al., 2024.)

Discrete Event Simulation (DES) stands as a computational modeling approach designed to analyze and comprehend the intricate dynamics of complex systems. Unlike continuous simulations, where changes unfold continuously over time, DES focuses on events that occur at distinct points in time, capturing the discrete nature of operations and interactions within a system. This is particularly relevant in well construction where rig state change and operational parameter

changes constitute discrete events. For further details on DES in this context, please refer to Naderi et al., 2024.

3.2 Utah FORGE Wellbore sections

This framework was applied to a simulation considering a coaxial well represented by concentric cylinders in 3D with mud flowing through the drill string and rising to the surface through the annular region between drill pipe and casing. The drill string components and casing program for sections using BHA 9 and BHA 18 referencing wellbore 16A(78)-32 are detailed in Table 1. The simulation encompasses a directional well trajectory, incorporating both vertical and horizontal sections.

Table 1: Basic data of drill string and casing program for wellbore 16A(78)-32.

Parameter	Inner diameter (mm)	Outer Diameter (mm)	Depth (m)
Drill Pipe	110	127	Variable
First Casing	220	240	1062.5
Second Casing	320	340	116.4
Third Casing	480	510	39.3

In configuring the model for evaluation and calibration using the Utah FORGE dataset, the static segment of the framework was defined from the surface down to the section corresponding to BHA 9 and 18 separately – the regions chosen for assimilation performance assessment. The raw data were trimmed and processed to enhance data quality and provide distinct case of continuous drilling operation for simplicity in model validation. Later, all operations in the respective BHA sections were considered. The time windows considered for sections BHA 9 and BHA 18 are clearly marked in Figure 5(a) and 6(a), respectively. As noted in the earlier sections, correct estimation of the initial conditions, i.e., the static model is important in simulating the temperature evolution through the dynamic model. This is reflected in the simulation results for BHA 9 and BHA 18. It can be noted from Figure 5(a) that by manipulating the initial estimate of geothermal gradient allowing for least error between the simulated and measured temperature profiles at the simulation start, the temperature dynamics follows the measurements. However, this is not the case when the input parameters are erratic as can be seen from Figure 5(b); although the initial conditions were manipulated in order to track the temperature dynamics at the later stage, there exists significant differences in the predicted and measured temperature in some regions. The initial state calibration was carried out through trial-and-error approach in this study but can be extended to an automatic calibration technique with ease. Similar observations can be noted for simulations in section BHA 18 as reflected in the Figure 6.

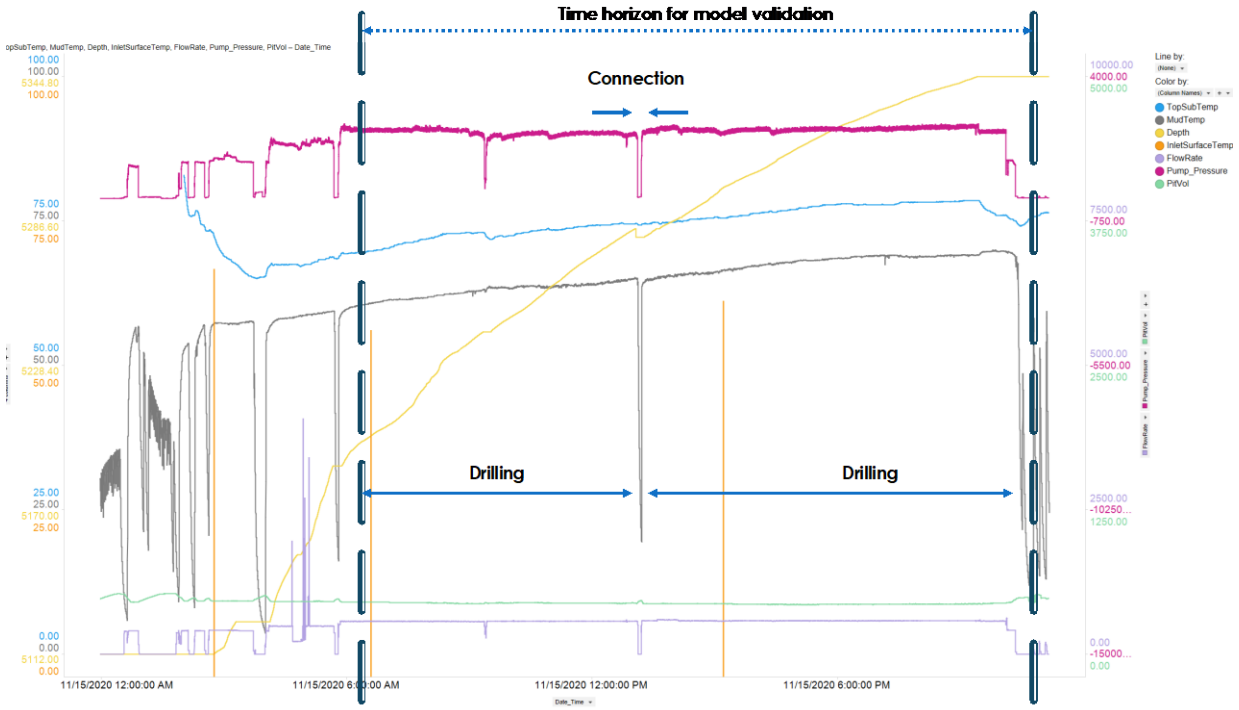

(a)

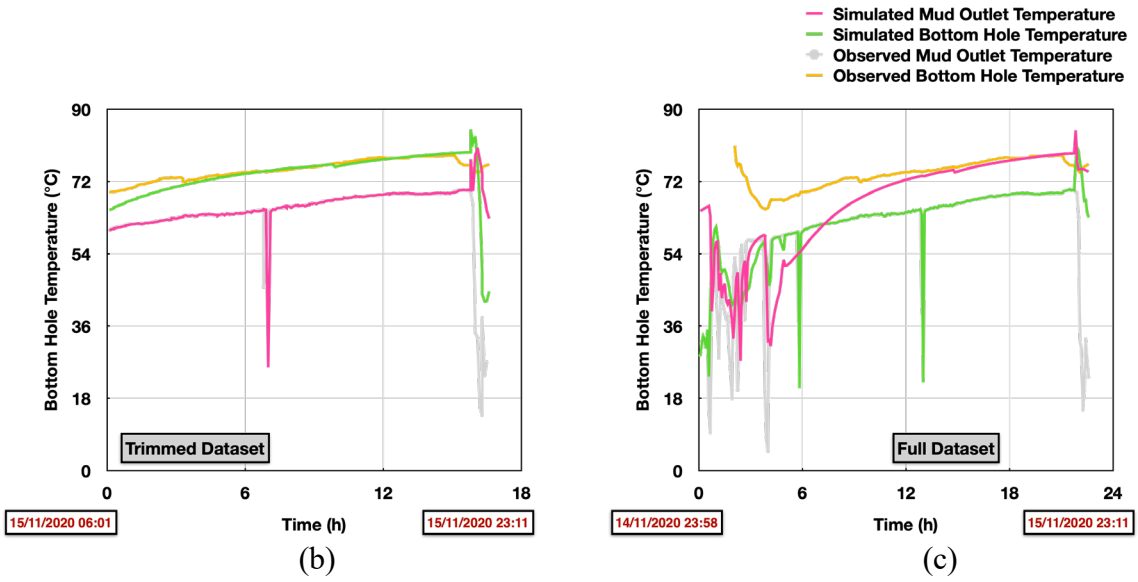

(b) (c)

Figure 5. (a) A selection of timeseries data from BHA 9 section of well 16A(78)-32 in Utah FORGE dataset; (b) Comparison of the time evolution of simulated and measured temperatures for a trimmed dataset for the section; and (c) Comparison of the time evolution of simulated and measured temperatures for full dataset for the section.

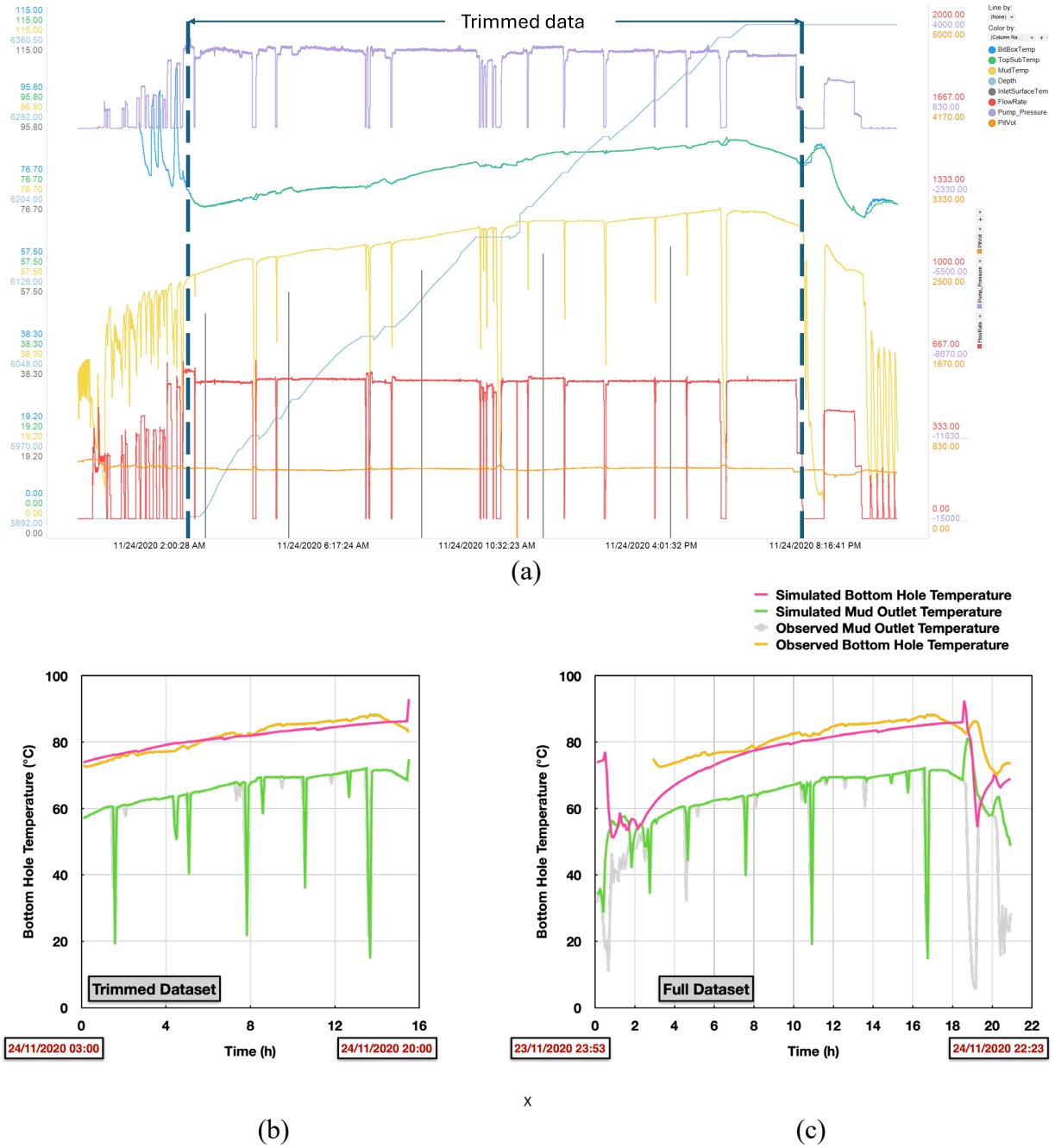

Figure 6. (a) A selection of timeseries data from BHA 18 section of well 16A(78)-32 in Utah FORGE dataset; (b) Comparison of the time evolution of simulated and measured temperatures for a trimmed dataset for the section; and (c) Comparison of the time evolution of simulated and measured temperatures for full dataset for the section.

4. Wellbore thermal management system

A hydrothermal simulator is an important tool for drilling geothermal wells offers important insights into the temperature distribution along the wellbore. It can be noted in the considered cases that the maximum temperature encountered in the wellbore are not always necessarily at the bottom. This is shown in the Figure 7 for two sections: nearly vertical BHA 9 and deviated BHA

18. The considered system generates the temperature profile along the wellbore depth at set time intervals, say every 5 minutes and provides information on the maximum temperature and the depth at which it is experienced. Given the computationally efficient model considered in this study, circulation rate and timing can be iterated over a certain interval to manage the wellbore temperature distribution accordingly. This information is crucial in cases like tripping in with downhole tools wherein they experience temperatures higher than their operational limit before they reach the bit is on-bottom. Thermal management becomes important to extend the operational lifetime of such tools and in avoiding significant NPT/ ILT due to downhole tool failures.

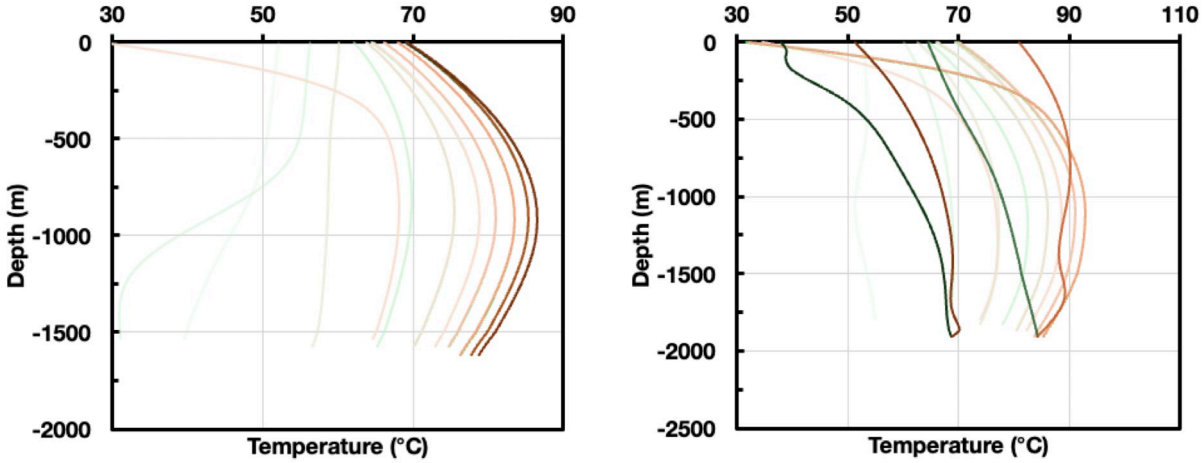

Figure 7. Time evolution (light to dark) of the temperature profile for the full dataset along the measured depth of the well for sections BHA 9 and BHA 18 of Utah FORGE well. Green line represents the temperature profile of mud inside drill string and brown the mud in annulus.

5. Conclusions

In this work, a computationally efficient hydrothermal model was developed to estimate the temperature distribution along the wellbore. The model has been updated from the authors' previous work to ensure numerical stability while handling real time data from the mud logging unit. The sensitivity analysis shows that the initial estimate of the geothermal gradient is important to follow the temperature dynamics of the system and that the gradient is not observable from the surface temperature as a measurement alone. Thus, bottom hole temperature measurements are necessary to calibrate the model through ML methods to accommodate the model uncertainties. The DES triggers the model to simulate temperature profile on system changes and the maximum temperature region is identified to inform on the mud circulation rate and time to allow for the downhole tool operations.

To build an automated thermal management system, further analysis of the controllability and the observability of the hydrothermal system is necessary. This shall pave way to designing an efficient controller for real time recommendation of the circulation rate and the circulation time for an optimized wellbore temperature profile.

Nomenclature

Abbreviations

BHA	Bottom Hole Assembly
DES	Discrete Event Simulation
FEM	Finite Element Model
FDM	Finite Difference Method
ML	Machine Learning
MPT	Mud Pulse Telemetry
NPT	Non-Productive Time
PIML	Physics-Informed Machine
3D	3 Dimensional
1D	1 Dimensional

Variables

R	Analogical thermal-electrical
h	Convective heat transfer
ρ	Density
Z	Depth
d	Diameter
f	Friction resistance coefficient
ΔP	Frictional resistance pressure
G	Geothermal gradient
q	Heat source term
D_h	Hydraulic diameter
r	Radius
Re	Reynolds number
c	Specific heat capacity
T	Temperature
λ	Thermal conductivity
t	Time
dt	Timestep
ν	Viscosity

Units

°C	Degree Celsius
K	Kelvin
kg	Kilogram
m	Meter
mm	Millimeter
Pa	Pascal
s	Second

Acknowledgement

The authors acknowledge the Utah FORGE project for the open dataset used in this study. The authors would like to thank Virgil Dynamics and Intellicess for granting permission to publish the results of their collaborative project in enhancing drilling performances in the geothermal industry.

REFERENCES

Chen, Z., & Novotny, R. J. (2003). Accurate prediction wellbore transient temperature profile under multiple temperature gradients: finite difference approach and case history. *SPE Annual Technical Conference and Exhibition.* (pp. SPE-84583) SPE .

Mitchell, R. F., & Miska, S. (2011). *Fundamentals of drilling engineering.*

Hasan, A. R., & Jang, M. (2021). An analytic model for computing the countercurrent flow of heat in tubing and annulus system and its application: Jet pump. *Journal of Petroleum Science and Engineering*, 203, 108492.

Polat, C. (2022). A semi-analytical solution technique for predicting circulating mud temperatures. *Journal of Natural Gas Science and Engineering*, 106, 104754.

Kshirsagar, A., & Sanghavi, P. (2022). Geothermal, oil and gas well subsurface temperature prediction employing machine learning. *47th workshop on geothermal reservoir engineering.*

Gonzalez Angarita, J. C. (2020). *Integrated Modelling and Simulation of Wellbore Heat Transfer Processes through High-level Programming, Sensitivity Analysis and Initial Approach with Machine Learning Predictive Models.* Norway: University of Stavanger.

Hasan, A. R., Kabir, C. S., & Sarica, C. (2018). *Fluid flow and heat transfer in wellbores.* Richardson, Texas, Richardson, Texas: Society of Petroleum Engineers.

Holmes, C. S., & Swift, S. C. (1970). Calculation of circulating mud temperatures . *Journal of petroleum technology*, 22(06), 670-674.

Zhang, Z., Xiong, Y., & Guo, F. (2018). Analysis of wellbore temperature distribution and influencing factors during drilling horizontal wells. *Journal of Energy Resources Technology*, 140(9), 092901.

Zhou, F. (2013). *Research on heat transfer in geothermal wellbore and surroundings.* Berlin.

Hasan, A. R., Kabir, C. S., & Wang, X. (2009). A robust steady-state model for flowing-fluid temperature in complex wells. *SPE Production & Operations*, 24(02), 269-276.

Merlo, A., Maglione, R., & Piatti, C. (1995). An innovative model for drilling fluid hydraulics. *SPE Asia Pacific Oil and Gas Conference and Exhibition* (pp. pp. SPE-29259). SPE.

Tekin, S. (2010). *Estimation of the formation temperature from the inlet and outlet mud temperatures while drilling geothermal formations* . Master's thesis, Middle East Technical University.

Brown, C. S., Cassidy, N. J., Egan, S. S., & Griffiths, D. (2021). Numerical modelling of deep coaxial borehole heat exchangers in the Cheshire Basin, UK. *Comuters & Geosciences*, 152, 104752.

Durst, F., & Arnold, I. (2008). *Fluid mechanics: an introduction to the theory of fluid flows.* Berlin: Springer.

Naderi, S., Velmurugan, N., Nannapaneni, P., Yi, M., & Ashok, P. An Integrated Data and Physics-based Temperature Model for Real-time Estimation of Bottomhole Temperature for Downhole Tool Failure Prevention.

Moura, C. A., & Kubrusly, C. S. (2012). *The Courant-Friedrichs-Lewy (CFL) condition: 80 years after its discovery. .* Basel: Birkhäuser.

Budgaga, W., Malensek, M., Pallickara, S., Harvey, N., Breidt, F. J., & Pallickara, S. (2016). Predictive analytics using statistical, learning, and ensemble methods to support real-time exploration of discrete event simulations. *Future Generation Computer Systems*, 56, 360-374.

Lang, S., Kuetgens, M., Reichardt, P., & Reggelin, T. (2021). Modeling production scheduling problems as reinforcement learning environments based on discrete-event simulation and openai gym. *IFAC* (pp. 54(1), 793-798). IFAC-PapersOnLine.

Kruszewski, M., & Wittig, V. (2018). Review of failure modes in supercritical geothermal drilling projects. *Geothermal Energy*, 6(1), 28.